nature medicine

Quantum dots spectrally distinguish multiple species within the tumor milieu *in vivo*

Mark Stroh[1], John P Zimmer[2], Dan G Duda[1], Tatyana S Levchenko[3], Kenneth S Cohen[4], Edward B Brown[1], David T Scadden[4], Vladimir P Torchilin[3], Moungi G Bawendi[2], Dai Fukumura[1] & Rakesh K Jain[1]

A solid tumor is an organ composed of cancer and host cells embedded in an extracellular matrix and nourished by blood vessels. A prerequisite to understanding tumor pathophysiology is the ability to distinguish and monitor each component in dynamic studies. Standard fluorophores hamper simultaneous intravital imaging of these components. Here, we used multiphoton microscopy techniques and transgenic mice that expressed green fluorescent protein, and combined them with the use of quantum dot preparations. We show that these fluorescent semiconductor nanocrystals can be customized to concurrently image and differentiate tumor vessels from both the perivascular cells and the matrix. Moreover, we used them to measure the ability of particles of different sizes to access the tumor. Finally, we successfully monitored the recruitment of quantum dot–labeled bone marrow–derived precursor cells to the tumor vasculature. These examples show the versatility of quantum dots for studying tumor pathophysiology and creating avenues for treatment.

Intravital microscopy has provided unprecedented molecular, cellular, anatomical and functional insight into tumor biology and response to treatment[1]. This technique captures fluorescence from molecules that are injected into a host or expressed by cells[2,3]. Additionally, intrinsic signals such as second harmonic generation (SHG) emanating from collagen can be imaged using multiphoton microscopy[4,5]. Traditional fluorophores are prone to photobleaching, compromising the ability to image the same region repeatedly, and have relatively narrow excitation and broad emission spectra. Also, several excitation wavelengths may be required to excite all fluorophores and intrinsic signals, and overlapping emissions may obscure the delineation between multiple probes. Quantum dots, colloidal semiconductor nanocrystals[6], have the potential to overcome these limitations: they are photostable, tunable to a desired narrow emission spectrum, relatively insensitive to the wavelength of excitation light, and are especially bright fluorophores[7]. Recent studies exploit these optical properties for imaging of cells[8] or whole tumors[9]. The ability of quantum dots to show crucial information at the length scale between these two extremes has yet to be established[10]. Here, we present studies that highlight the synergy of quantum dots and multiphoton intravital microscopy for tumor pathophysiology studies: differentiating tumor vessels from both perivascular cells and matrix, assaying the ability of microparticles to access the tumor, and monitoring the trafficking of precursor cells.

RESULTS

Customizing quantum dot emission

Because quantum dot emissions are tunable by both size and chemical composition[6], we prepared three types of quantum dots with spectra that overlapped minimally both with each other and with the emissions from green fluorescent protein (GFP) and SHG (**Fig. 1a**). The quantum dot with a 470 nm emission maximum (QD470) lies in between the SHG and GFP signals and was composed of a CdS core overcoated with a ZnS passivating shell[11] and tri-*n*-octylphosphine oxide (TOPO) surface ligands protected the quantum dots from agglomeration. The other two quantum dots emitted redder wavelengths than GFP and differed in composition from the blue quantum dot. The quantum dots with 590 nm and 660 nm emission maxima (QD590 and QD660, respectively) shared the same core, passivating shell and ligands comprised of CdSe[12], $Zn_{0.8}Cd_{0.2}S$ alloy and TOPO, respectively, but differed in the size of the core; the larger core showed the redder emission. In this fashion, we customized the quantum dot fluorescence to avoid the fixed signals emanating from the tumor environment and gained the ability to excite several species concurrently because of the broad two-photon action cross-sections (**Fig. 1b**).

Differentiating tumor vessels from perivascular cells and matrix

The blood vessel wall consists of endothelial cells and perivascular cells embedded in a collagen IV–rich basement membrane. In tumors, these vessels are tortuous, dilated and leaky. Both the perivascular cells and the basement membrane are absent or abnormal, and the components of the vessel wall change both spatially within a tumor and temporally with tumor growth and treatment. Because most information about the interaction among these components has come from immunohistochemical

[1]E.L. Steele Laboratory for Tumor Biology, Department of Radiation Oncology, Massachusetts General Hospital and Harvard Medical School, 100 Blossom Street, Boston, Massachusetts 02114, USA. [2]Department of Chemistry, Massachusetts Institute of Technology, 77 Massachusetts Avenue, Cambridge, Massachusetts 02139, USA. [3]Department of Pharmaceutical Sciences, Northeastern University, 312 Mugar Hall, Boston, Massachusetts 02115, USA. [4]Center for Regenerative Medicine and Technology, Massachusetts General Hospital, 13th Street, Charlestown, Massachusetts 02129, USA. Correspondence should be addressed to R.K.J. (jain@steele.mgh.harvard.edu).

Published online 8 May 2005; doi:10.1038/nm1247

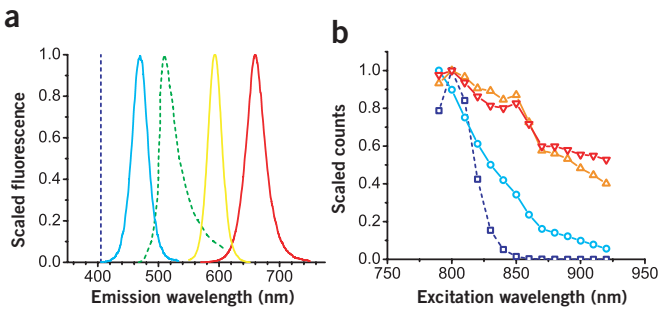

Figure 1 Spectra corresponding to representative quantum dots used in this study. (**a**) The family of emission spectra was generated from quantum dots tuned to emit at wavelengths not shared by signals from GFP and second harmonic generation (green and dark blue dashed lines, respectively). In this depiction, second harmonic generation is generated with 810-nm incident light. The quantum dot emission spectra were narrow and symmetric; corresponding emission peaks and associated full-width half-maximum values were 470 and 30, 590 and 30, and 660 and 40 nm for QD470 (light blue line), QD590 (orange line) and QD660 (red line), respectively. (**b**) The relative two-photon action cross-sections (scaled to a maximum value of 1) for the corresponding quantum dot and cascade blue (dark blue line). Owing to the relatively broad two-photon action cross sections, the quantum dot may be excited concomitantly with the intrinsic second harmonic generation and GFP sources using multiphoton microscopy.

studies of excised tissue, there is a paucity of dynamic information. To this end, we developed a transgenic mouse in which the perivascular cells express GFP under the control of the vascular endothelial growth factor (VEGF) promoter (VEGF-GFP)[3]. Although this potentially allows us to visualize both the perivascular cells and blood vessels *in vivo*, fluorescently labeled dextrans, commonly infused to highlight tumor vessels, leak into the extravascular space and blur the boundary of the vessel wall. To illustrate this point, we highlighted tumor vessels with a dextran that has a molecular weight of 2,000,000 conjugated to cascade blue (Molecular Probes). After infusion into a transgenic VEGF-GFP mouse bearing a MCaIV tumor subcutaneously in a dorsal skinfold chamber[1], we imaged the tumor vessels using multiphoton microscopy. The dextran conjugate extravasated and readily entered the tumor interstitium within 30 min, and the vessel wall was obscured (**Fig. 2a** and **Supplementary Movie 1** online). Numerous reports conclude that extended, flexible molecules generally experience reduced hindrance to interstitial transport relative to more spherical and rigid counterparts[13]; accordingly, we reasoned that quantum dots would not collect in the interstitium as readily and therefore provide a sharper boundary at the vessel wall. We encapsulated quantum dots in *n*-poly (ethylene glycol) phosphatidylethanolamine (PEG-PE, Avanti Polar Lipids) to render quantum dots stable under physiological conditions[14]. We administered the QD470 micelle to an identical animal model as investigated before with labeled dextran; the QD470 provided a sharp boundary between intra- and extravascular spaces (**Fig. 2b** and **Supplementary Movie 2** online). Whereas the dextran extravasated and entered the tumor in under 30 min, quantum dots showed no similar behavior over similar timescales for MCaIV and other tumor types (**Supplementary Fig. 1** online). Additionally, because GFP is optimally excited at wavelengths beyond 850 nm[4], the relatively broad excitation spectrum of QD470 relative to cascade blue (**Fig. 1b**) permitted concurrent excitation of both quantum dots and GFP. As shown, QD470 and GFP were concurrently excited with 850 nm light to show sharply demarcated vessels and crisscrossing GFP-expressing perivascular cells (**Fig. 2c**).

In addition to perivascular cells, the extracellular matrix affects tumor pathophysiology and drug delivery. After systemic administration, drugs first cross the vessel wall and then navigate the collagen I–rich interstitium; the arrangement of vessels in this matrix is therefore a key determinant of how efficiently drugs infiltrate the mass. Recently, SHG has allowed imaging of collagen in tumors[5]. Because SHG requires relatively high-power incident light, imaging both vessels and collagen requires photostable plasma markers. Also, the SHG signal is collected at half the wavelength of the incident light, and protein autofluorescence emits up to the 500 nm range; thus, a red intravascular marker with narrow emission avoids cross-talk between collagen signal and intravascular dye. Accordingly, a wild-type C3H mouse bearing a MCaIV tumor in a skinfold chamber was infused with a QD660 micelle preparation; tumor vessels were highlighted with far-red emitting QD660, whereas the SHG signal was collected at 405 nm (**Fig. 2d**). The broad excitation spectrum and high photostability of quantum dots permitted simulta-

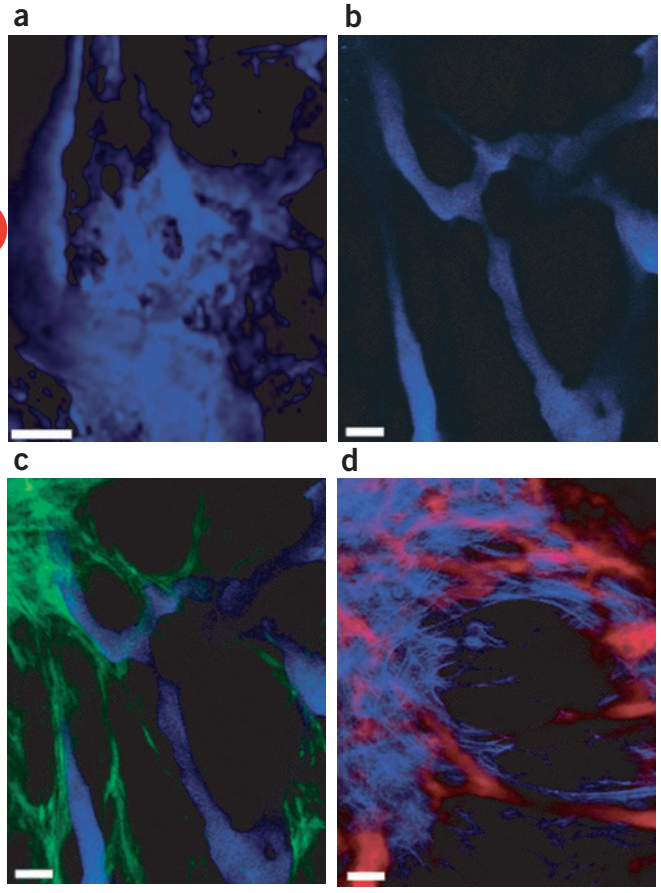

Figure 2 Vascular imaging with quantum dots. (**a**) The depth projection of 20 images taken at 5-μm intervals depicts pockets of labeled dextrans that have extravasated and collected in the interstitium, resulting in blurred tumor vessels. (**b**) When QD470 is used as a vessel marker, the depth projection of 15 images obtained at 5-μm intervals shows a sharp boundary between vessel and interstitium. (**c**) Concurrent imaging of both QD470 and GFP (indicated in green) provides clear separation of vessel from GFP-expressing perivascular cells. (**d**) Vessels highlighted with a deep red (QD660) micelle preparation were imaged simultaneously with the SHG signal (indicated in blue); the image represents a projection of a stack of 20 images at an interval of 2 μm per slice. Scale bar, 50 μm.

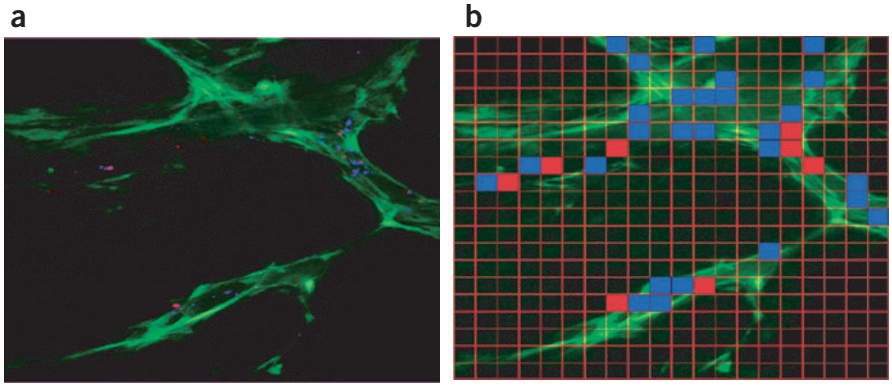

Figure 3 Quantum dot–loaded beads as drug delivery vehicle. Both 100 and 500 nm silica microspheres were loaded with QD470 and QD590, respectively, and administered to a VEGF-GFP mouse bearing a MCaIV tumor explant in a skinfold chamber. (**a**) After a 5-h period, a depth projection of five images taken at 5-μm intervals showed a heterogeneous extravasation pattern. (**b**) This image was meshed with a 20 × 20 grid, and regions that correspond to a maximum extravasated particle size of 500 nm and 100 nm are indicated with red and blue grids, respectively. In this fashion, we assessed the ability of candidates to access VEGF-GFP perivascular cells. The image is 707 μm across.

neous excitation and collection of light spanning the visible spectrum. Because the SHG signal and QD660 emissions were so widely spaced, and the quantum dot emission was narrow (full-width half-maximum value of 40 nm for this quantum dot), emission cross-talk with the SHG channel was minimized. Similar to GFP-expressing stromal cells, the collagen, which was juxtaposed and crossed over the vasculature, was clearly discernable from the vessel. Thus, quantum dots are stable, bright, robust chromaphores for anatomical imaging, providing sharp delineation of both perivascular cells and matrix from blood vessels.

Assaying the ability of particles to access the tumor

Particulate drug delivery vehicles for cancer therapy are on the order of hundreds of nanometers[1,15]. Although larger particulate systems may provide a more substantial drug depot or allow for more sophisticated design, those beyond the size of pores in the vessel wall are excluded from targets within the tumor. Little is known about local heterogeneity in the effective pore size cut-off of vessels and how this might impact the ability of particles to access targets[15]. Because conventional fluorophores have broad emission spectra, it is difficult to distinguish among several probes administered concurrently; further, spectral overlap with a population of fluorescence-emitting target cells obscures delineation of particle from target. To circumvent these difficulties, we utilized quantum dot–tagged silica microspheres in conjunction with multiphoton intravital microscopy as a new method to guide the design of particulate drug delivery vehicles. Here, we assayed for the ability of differently sized quantum dot–encoded microspheres to access VEGF-GFP perivascular cells. Following a recent protocol[16], we prepared highly uniform 100 nm and 500 nm silicate beads, which were loaded with QD470 and QD590, respectively. The quantum dot–encoded spheres were administered concurrently to a VEGF-GFP mouse bearing a MCaIV tumor in a skinfold chamber. Following a 5-h period of extravasation, we imaged a region of the tumor to show the distribution of microspheres (**Fig. 3a**). By tuning the quantum dot fluorescence from the GFP emission, we could assess the ability of multiple candidates to access the perivascular cells. First, images corresponding to 500 nm and 100 nm spheres were binarized to show extravasated beads using Matlab's Image Processing Toolbox (Mathworks). We next partitioned the image into a 20 × 20 grid (**Fig. 3b**); grids containing a maximum bead size of 500 nm and 100 nm were colored red and blue, respectively. This depiction shows zones accessible to the 500-nm candidate (red squares), as well as those restricted to only the smaller 100-nm candidate (blue squares). Additionally, this method may guide further vehicle optimization. For example, a new assay with probes sized between 100 nm and 500 nm would prove useful if one sought to maximize both the size of the depot and the uniformity of the particle distribution.

Tracking bone marrow–derived cells

Tissue neovascularization involves both the participation of local endothelial cells and the recruitment of circulating progenitor cells[17,18]. The mechanism of homing of the bone marrow–derived

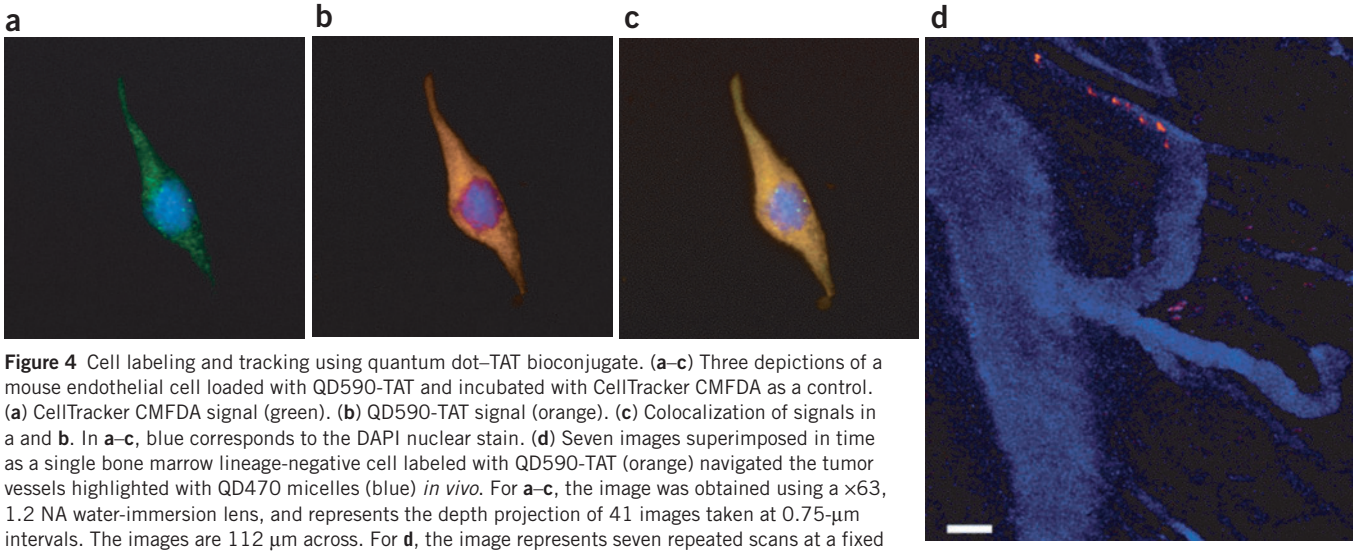

Figure 4 Cell labeling and tracking using quantum dot–TAT bioconjugate. (**a**–**c**) Three depictions of a mouse endothelial cell loaded with QD590-TAT and incubated with CellTracker CMFDA as a control. (**a**) CellTracker CMFDA signal (green). (**b**) QD590-TAT signal (orange). (**c**) Colocalization of signals in a and **b**. In **a**–**c**, blue corresponds to the DAPI nuclear stain. (**d**) Seven images superimposed in time as a single bone marrow lineage-negative cell labeled with QD590-TAT (orange) navigated the tumor vessels highlighted with QD470 micelles (blue) *in vivo*. For **a**–**c**, the image was obtained using a ×63, 1.2 NA water-immersion lens, and represents the depth projection of 41 images taken at 0.75-μm intervals. The images are 112 μm across. For **d**, the image represents seven repeated scans at a fixed depth (~100 μm) taken at 1-s intervals. Scale bar, 50 μm.

cells and the extent to which their recruitment contributes to tumor neovascularization has become a subject of intense debate[19]. Multiphoton intravital microscopy is well suited for tracking cells *in vivo*, but the relationship between single- and two-photon absorption spectra is not obvious, complicating the use of multiphoton microscopy with common dyes for cell tracking[20]. Further, common fluorophores and fluorescent proteins may suffer photobleaching with repeated scanning, and spectral separation of cells from the plasma marker is hampered because of broad emissions. In this study, we exploited the optical properties of quantum dots to circumvent these limitations. First we encapsulated QD590 using a mixture of PEG-PE with 3–10% of a PEGylated lipid covalently coupled to the human immunodeficiency virus TAT protein through a *p*-nitrophenylcarbonyl spacer[21] (QD590-TAT). Recent studies highlight the use of TAT peptides for loading progenitor cells with magnetic nanoparticles[22], and for labeling cancer cells with quantum dots[9]. Accordingly, we next used the QD590-TAT conjugate to label mouse endothelial cells, and CellTracker CMFDA as a control (**Fig. 4a–c** and **Supplementary Movie 3** online). These images, representative of the robust labeling by QD590-TAT for the entire population of cells, show that the QD590-TAT signals colocalized with those from CMFDA. For *in vivo* studies, primary bone marrow lineage-negative cells, a population enriched in progenitor and stem cells, were isolated as described previously[23] and incubated with QD590-TAT. We infused both QD470 micelles and the *ex vivo*–labeled lineage-negative cells through the carotid artery of a mouse bearing a MCaIV tumor in a cranial window preparation; we imaged the blood flow and rolling and adhesion of lineage-negative cells to tumor endothelium with 800 nm light (**Fig. 4d**). The ability to contemporaneously excite and monitor both quantum dots avoided difficulties with registration as a result of sequential monitoring with multiple wavelengths, and the bright, nonoverlapping quantum dot emissions enabled clear differentiation of cell from plasma marker.

DISCUSSION

Multiphoton microscopy provides *in vivo* imaging with high spatial resolution, but concurrent imaging of multiple species is difficult with standard fluorophores. In this study, we have shown that the strengths of quantum dots match the demands inherent to intravital microscopy. The quantum dots are flexible fluorescent probes that can be excited concurrently with, and tuned away from, signals resulting from GFP and SHG. Unlike dextran conjugates that collect within the interstitium[24] and impede clean demarcation of the vessel wall, the use of quantum dots as extrinsic fluorophores allows vessels to be both morphologically and spectrally distinct.

This work also shows the utility of the new, robust quantum dot–microsphere composites for optimizing delivery vehicles. As noted previously[16], the procedure used to prepare these materials enables preparation of a wide range of monodisperse submicron sphere sizes. The ability to tune not only the size but also the surface characteristics of these quantum dot composites through silica chemistry provides an additional handle for screening a large number of drug delivery parameters for targeting efficacy. Moreover, the use of multiphoton intravital microscopy with these fluorescent materials shows local inhomogeneities in both tumor components and delivery; information that is not provided by tumor-averaged techniques[9]. Similarly, for cell trafficking studies, one may use different quantum dots to label subpopulations of bone marrow–derived cells (or progenitor cells isolated from different mutant animals) to investigate the degree to which the vascular and perivascular structures are formed or remodeled in response to cell homing.

Introducing this technology to a clinical setting will depend crucially upon biocompatibility and safety of the quantum dot formulation. The micelle quantum dot preparation used in this study was previously shown to be nontoxic to developing *Xenopus* embryos[14]. Several studies indicate that other encapsulation chemistries render quantum dots biocompatible in cell culture[25]. Of note, we infused nanomole quantities of quantum dot preparations in mice and noted no obvious adverse effects for up to 1 month. Thus, we may someday exploit the special synergy of multiphoton intravital microscopy and quantum dots as a clinical diagnostic and prognostic tool for cancer prevention and treatment.

METHODS

Quantum dot synthesis and characterization. The quantum dot cores used in this study were prepared as described previously[11,12]. The CdS quantum dots were overcoated with a ZnS passivating layer[11,26,27] whereas the CdSe quantum dots were overcoated using a $Zn_{0.8}Cd_{0.2}S$ layer (P.T. Snee, Y. Chan & M.G.B., unpublished data). We obtained the quantum dot absorption and emission spectra using a Hewlett-Packard 8452 diode array UV-vis spectrometer and a SPEX Fluorolog 1680 spectrometer, respectively. The quantum dots were rendered water soluble and biocompatible through encapsulation in PEGylated phospholipid micelles[14]. For the quantum dot–TAT conjugates, we used an identical procedure, except 3–10% of the PEG-PE was substituted with a TAT-conjugated lipid described elsewhere[21].

Quantum dot–microsphere composite synthesis and characterization. The quantum dot–encoded silica microspheres were synthesized according to a recently developed procedure[16]. Briefly, we added 10 µl of a solution of QD470 or QD590 dispersed in ethanol through cap exchange with 5-amino-1-pentanol and 3-aminopropyltrimethoxysilane to 30 mg silica microspheres (previously synthesized by the Stöber process or purchased from Polysciences) and 16 mg hydroxypropyl cellulose (average MW = 370,000) dispersed in 10 ml of vigorously stirred ethanol, followed by the addition of 50 µl H_2O, 50 µl NH_4OH (28% in H_2O) and 0.15 ml tetraethoxysilane. We then immersed the mixture in an oil bath at 75 °C for 4 h and continued to stir. The quantum dot–microsphere composites were then isolated by 3–4 cycles of centrifugation to precipitate followed by redispersal in ethanol. Dried spheres were then PEGylated by treatment with 3-aminopropyltriethoxysilane in acetone followed by overnight stirring in *N,N*-dimethylformamide with mPEG-NHS (MW = 2,000). Solvent exchange with PBS yielded the final materials.

Cell culture and quantum dot–TAT loading. All cell culture media and supplements were purchased from Invitrogen. We maintained mouse endothelial cells (MS1 cells; ATCC) in DMEM supplemented with 10% FBS. Before incubation with QD590-TAT, the endothelial cells were transferred to chamber slides (BD Falcon), and a fraction of these cells was incubated with 5-chloromethylfluorescein diacetate (CellTracker Green CMFDA, Molecular Probes) following the manufacturer's instructions. After marrow harvest from mice (β-actin-GFP/C57BL/6/Osb acquired from Jackson Laboratories and subsequently bred in our animal facility), we isolated lineage-negative bone marrow cells as previously described[23] and maintained them in RPMI medium supplemented with 2% FBS on ice until subsequent loading with QD590-TAT. Both cell populations were incubated with 4 µM QD590-TAT for 1–2 h at 37 °C in serum-free media. The endothelial cells were then washed extensively with PBS, fixed with 4% paraformaldehyde, washed again and mounted on glass slides using Vectashield mounting medium with DAPI (Vector Laboratories). For the lineage-negative cells, we washed the cells twice after incubation the cells with RPMI medium supplemented with 2% FBS. Because the lineage-negative cells were isolated from β-actin-GFP mice, we could readily confirm loading of the cells using multiphoton microscopy and epifluorescence microscopy resulting from the colocalized GFP and QD590 signal. After this confirmation, we infused 400,000 cells locally in the tumor through a carotid cannula.

Animal preparations and imaging. We conducted animal experiments with the approval of the Massachusetts General Hospital Subcommittee on Research Animal Care. Animals were anesthetized with ketamine and xylazine (100/10 mg/kg, intramuscularly) for all procedures. We grew isogenic mouse mammary adenocarcinoma MCaIV tumor explants subcutaneously in C3H mice (wild-

type or VEGF-GFP transgenic) bearing dorsal skinfold chambers[28]. In separate experiments, we grew MCaIV and U87 glioma on the surface of the brain of SCID mice with cranial window preparations[29]. Quantum dot and cell infusions were administered either systemically through the lateral tail vein or locally through the carotid artery; cannulation of the carotid artery was performed immediately before *in vivo* tracking studies[30]. We acquired images using custom-built multiphoton microscopes. One multiphoton microscope is described elsewhere[2], and the other consisted of a modified Fluoview confocal scanhead (Olympus) and a Mai Tai Femtosecond Ti:sapphire laser (Spectra Physics). Nondescanned detection was performed with HC125-02 photomultiplier tubes (Hamamatsu Photonics). We collected the signals from second harmonic generation, QD470, GFP, QD590 and QD660 using 405DF30, D470/40, D535/40, D605/55 and D650/40 detection filters, respectively (Chroma Technology).

Note: Supplementary information is available on the Nature Medicine website.

ACKNOWLEDGMENTS

We thank J. Kahn and S. Roberge for their assistance with the animal preparations. We wish to acknowledge Y.T. Chan, P. Snee, J.S. Steckel and J.B. Tracy for their help with quantum dot synthesis, and R.J. Klein for the separation of bone marrow lineage-negative cells. This work was supported by a National Cancer Institute fellowship to M.S. (F32 CA103386), a US National Institutes of Health grant (5RO1 EB001961-06) to V.T., and a Bioengineering Research Partnership Grant (R24CA85140) and Program Project Grant (P01CA80124) to R.K.J. and D.F. This work was also supported by grants to M.G.B. from the National Science Foundation (NSF-CHE-020989) and the Army Research Office through the Institute for Collaborative Biotechnologies. D.G.D. is a Cancer Research Institute fellow.

COMPETING INTERESTS STATEMENT

The authors declare that they have no competing financial interests.

Received 27 August; accepted 12 December 2004
Published online at http://www.nature.com/naturemedicine/

1. Jain, R.K., Munn, L.L. & Fukumura, D. Dissecting tumour pathophysiology using intravital microscopy. *Nat. Rev. Cancer* **2**, 266–276 (2002).
2. Brown, E.B. *et al*. *In vivo* measurement of gene expression, angiogenesis and physiological function in tumors using multiphoton laser scanning microscopy. *Nat. Med.* **7**, 864–868 (2001).
3. Fukumura, D. *et al*. Tumor induction of VEGF promoter activity in stromal cells. *Cell* **94**, 715–725 (1998).
4. Zipfel, W.R., Williams, R.M. & Webb, W.W. Nonlinear magic: multiphoton microscopy in the biosciences. *Nat. Biotechnol.* **21**, 1369–1377 (2003).
5. Brown, E. *et al*. Dynamic imaging of collagen and its modulation in tumors *in vivo* using second-harmonic generation. *Nat. Med.* **9**, 796–800 (2003).
6. Murray, C.B., Norris, D.J. & Bawendi, M.G. Synthesis and characterization of nearly monodisperse CdE (E = S, Se, Te) semiconductor nanocrystallites. *J. Am. Chem. Soc.* **115**, 8706–8715 (1993).
7. Larson, D.R. *et al*. Water-soluble quantum dots for multiphoton fluorescence imaging *in vivo*. *Science* **300**, 1434–1436 (2003).
8. Wu, X. *et al*. Immunofluorescent labeling of cancer marker Her2 and other cellular targets with semiconductor quantum dots. *Nat. Biotechnol.* **21**, 41–46 (2003).
9. Gao, X., Cui, Y., Levenson, R.M., Chung, L.W. & Nie, S. *In vivo* cancer targeting and imaging with semiconductor quantum dots. *Nat. Biotechnol.* **22**, 969–976 (2004).
10. Jain, R.K. & Stroh, M. Zooming in and out with quantum dots. *Nat. Biotechnol.* **22**, 959–960 (2004).
11. Steckel, J.S. *et al*. Blue luminescence from (CdS)ZnS core-shell nanocrystals. *Angewandte Chemie-International Edition* **43**, 2154–2158 (2004).
12. Fisher, B.R., Eisler, H.J., Stott, N.E. & Bawendi, M.G. Emission intensity dependence and single-exponential behavior in single colloidal quantum dot fluorescence lifetimes. *J. Phys. Chem. B* **108**, 143–148 (2004).
13. Pluen, A., Netti, P.A., Jain, R.K. & Berk, D.A. Diffusion of macromolecules in agarose gels: Comparison of linear and globular configurations. *Biophys. J.* **77**, 542–552 (1999).
14. Dubertret, B. *et al*. *In vivo* imaging of quantum dots encapsulated in phospholipid micelles. *Science* **298**, 1759–1762 (2002).
15. Hobbs, S.K. *et al*. Regulation of transport pathways in tumor vessels: role of tumor type and microenvironment. *Proc. Natl. Acad. Sci. USA* **95**, 4607–4612 (1998).
16. Chan, Y.T. *et al*. Incorporation of luminescent nanocrystals into monodisperse core-shell silica microspheres. *Adv. Mater.* **16**, 2092–2097 (2004).
17. Carmeliet, P. & Jain, R.K. Angiogenesis in cancer and other diseases. *Nature* **407**, 249–257 (2000).
18. Rafii, S., Lyden, D., Benezra, R., Hattori, K. & Heissig, B. Vascular and haematopoietic stem cells: novel targets for anti-angiogenesis therapy? *Nat. Rev. Cancer* **2**, 826–835 (2002).
19. Jain, R.K. & Duda, D.G. Role of bone marrow-derived cells in tumor angiogenesis and treatment. *Cancer Cell* **3**, 515–516 (2003).
20. Bestvater, F. *et al*. Two-photon fluorescence absorption and emission spectra of dyes relevant for cell imaging. *J. Microsc.* **208**, 108–115 (2002).
21. Torchilin, V.P., Rammohan, R., Weissig, V. & Levchenko, T.S. TAT peptide on the surface of liposomes affords their efficient intracellular delivery even at low temperature and in the presence of metabolic inhibitors. *Proc. Natl. Acad. Sci. USA* **98**, 8786–8791 (2001).
22. Lewin, M. *et al*. Tat peptide-derivatized magnetic nanoparticles allow *in vivo* tracking and recovery of progenitor cells. *Nat. Biotechnol.* **18**, 410–414 (2000).
23. Cheng, T. *et al*. Hematopoietic stem cell quiescence maintained by p21cip1/waf1. *Science* **287**, 1804–1808 (2000).
24. Koike, N. *et al*. Tissue engineering: creation of long-lasting blood vessels. *Nature* **428**, 138–139 (2004).
25. Jaiswal, J.K., Mattoussi, H., Mauro, J.M. & Simon, S.M. Long-term multiple color imaging of live cells using quantum dot bioconjugates. *Nat. Biotechnol.* **21**, 47–51 (2003).
26. Hines, M.A. & Guyot-Sionnest, P. Synthesis and characterization of strongly luminescing ZnS-Capped CdSe nanocrystals. *J. Phys. Chem.* **100**, 468–471 (1996).
27. Dabbousi, B.O. *et al*. (CdSe)ZnS core-shell quantum dots: synthesis and characterization of a size series of highly luminescent nanocrystallites. *J. Phys. Chem. B* **101**, 9463–9475 (1997).
28. Leunig, M. *et al*. Angiogenesis, microvascular architecture, microhemodynamics, and interstitial fluid pressure during early growth of human adenocarcinoma LS174T in SCID mice. *Cancer Res.* **52**, 6553–6560 (1992).
29. Yuan, F. *et al*. Vascular permeability and microcirculation of gliomas and mammary carcinomas transplanted in rat and mouse cranial windows. *Cancer Res.* **54**, 4564–4568 (1994).
30. Melder, R.J., Salehi, H.A. & Jain, R.K. Interaction of activated natural killer cells with normal and tumor vessels in cranial windows in mice. *Microvasc. Res.* **50**, 35–44 (1995).